THE JOURNAL OF PHYSICAL CHEMISTRY C

Article

pubs.acs.org/JPCC

Dual-Sensitization via Electron and Energy Harvesting in CdTe Quantum Dots Decorated ZnO Nanorod-Based Dye-Sensitized Solar Cells

Soumik Sarkar,[†] Abhinandan Makhal,[†] Karthik Lakshman,[‡] Tanujjal Bora,[‡] Joydeep Dutta,[‡,§] and Samir Kumar Pal*,[†]

[†]Department of Chemical, Biological and Macromolecular Sciences, S. N. Bose National Centre for Basic Sciences, Block JD, Sector III, Salt Lake, Kolkata 700 098, India

[‡]Centre of Excellence in Nanotechnology, School of Engineering and Technology, Asian Institute of Technology, Klong Luang, Pathumthani 12120, Thailand

[§]Chair in Nanotechnology, Water Research Center, Sultan Qaboos University, P.O. Box 17, 123 Al-Khoudh, Sultanate of Oman

ABSTRACT: Different-sized, 3-mercaptopropionic acid (MPA) stabilized CdTe quantum dots (QDs) have been prepared in aqueous solution, and potential cosensitization of such QDs in ZnO nanorod (NR)-based dye-sensitized solar cells (DSSCs) has been established. The results presented in this study highlight two major pathways by which CdTe QDs may contribute to the net photocurrent in a DSSC: (1) a direct injection of charge carriers from QDs to ZnO semiconductor via photoinduced electron transfer (PET) and (2) an indirect excitation of the sensitizing dye (SD) N719 molecules by funneling harvested light via Förster resonance energy transfer (FRET). The steady-state and picosecond-resolved luminescence measurements were combined to clarify the process of PET and FRET from the excited QDs to ZnO NR and SD N719, respectively. On the basis of these advantages, the short-circuit current density and the photoconductivity of the QD-assembled DSSCs with distinct architectures are found to be much higher than DSSCs fabricated with N719 sensitizer only.

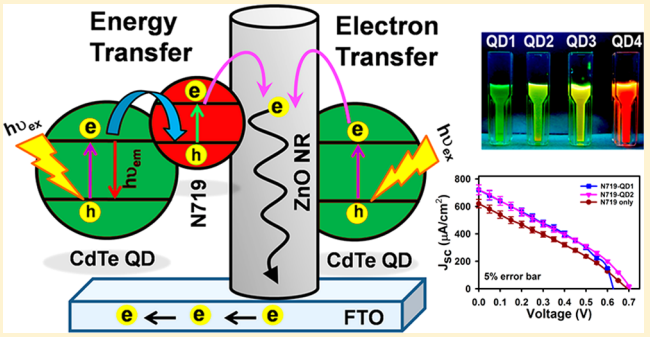

1. INTRODUCTION

Dye-sensitized solar cells (DSSCs) are based on solar light harvesting through the sensitizing dye (SD) attached to a wide band gap semiconductor first introduced by O'Regan and Grätzel.[1] The SD is an essential constituent in nanocrystalline DSSCs that has a potential for future photovoltaic applications owing to the lower fabrication costs of solar cells with acceptable conversion efficiencies.[1,2] The most successful and widely used dyes employed in DSSCs are ruthenium complexes,[3−5] ($Ru(dcbpy)_2(NCS)_2$), N_3 (dcbpy = 4,4-dicarboxy-2,2′-ipyridine), and bistetrabutylammonium salt N719, which have fairly broad optical absorption spectra ($\Delta\lambda \approx 350$ nm) but low molar extinction coefficients (5000−20 000 M^{-1} cm^{-1}). Alternative organic dyes have recently been developed with substantially higher molar extinction coefficients (50 000−200 000 M^{-1} cm^{-1}) but show narrow spectral bandwidths ($\Delta\lambda \approx 250$ nm).[6−8] Dye cocktails lead to a broader absorption spectra,[9] but because of the absence of dyes that absorb efficiently in the red part of the spectrum, generally a lower efficiency is achieved. As dyes with strong absorptivity do not typically exhibit broad absorption overlapping the solar spectra, this is one of the major pitfalls of using dyes as photosensitizers in solar cells.

Many efforts have been made to introduce stronger light absorber and to widen the spectral response of the photosensitizers. In recent times, the use of QDs as light harvesters has stimulated a lot of interest because of its higher extinction coefficient compared to conventional dyes[10] for efficient light energy conversion.[11−14] Because of the size quantization property, the optical and electronic properties of the semiconductor QDs can be engineered to further tune the response of quantum dot solar cells (QDSCs).[15−17] In addition, QDs open up new possibilities for the utilization of hot electrons[18] or multiple charge carrier generation with a single photon.[19] Multiple carrier generation in PbSe nanocrystals has shown that two or more excitons can be generated with a single photon of energy greater than the band gap.[20] The performance of a QDSC is currently limited by several factors, including a limited choice of electrolytes with which QDs are chemically compatible, insufficient passivation of recombination channels (usually attributed to surface traps), and limited QD loading capacities.[21] Recent studies have shown that it is possible to

Received: May 14, 2012
Revised: June 13, 2012
Published: June 14, 2012

dx.doi.org/10.1021/jp3046593 | J. Phys. Chem. C 2012, 116, 14248−14256

stabilize CdS QD-based DSSCs by coating the QD-sensitized nanoporous electrodes with a thin amorphous TiO_2 layer which enables the use of various QD sensitizers in the presence of iodine-based electrolytes.[22] Utilizing two sensitizing layers of SD N719 and CdS QDs separated by an amorphous titanium dioxide (TiO_2) layer, a significant increase in cell efficiency compared to a QD monolayer cell has been reported.[23] In a more recent study, Etgar et al. have used a cobalt complex (Co^{2+}/Co^{3+}) as an electrolyte in the cells which permits direct contact between the QDs and the electrolyte.[24] Choi et al. have recently demonstrated the coupling of semiconductor nanocrystal and a red-NIR organic dye with complementary spectral absorption in the visible region.[25]

Utilization of two sensitizers (one acting as energy donor while the other as an acceptor) can be very useful in order to achieve both broadening of optical absorption region in DSSCs as well as increasing the absolute loading of absorbing media on the semiconductor. This novel approach is based on Förster resonance energy transfer (FRET) which has recently experienced a significant interest of several groups[24,26−30] including ours.[31,32] The use of FRET between covalently linked energy donor molecules to the SD which are attached to the semiconductor (titania) surface has been demonstrated in the literature[33] where higher excitation transfer efficiency (>89%) between attached dye molecules and a subsequent improvement in the device external quantum efficiency of 5−10% between 400 and 500 nm spectral range has been reported. The overall enhancement of power conversion efficiency of the DSSC was still low (<9%), which was argued to arise because of an increase in the open-circuit voltage rather than because of an increase in the short-circuit photocurrent density. Recently, it has been demonstrated that unattached, highly luminescent chromophores inside a liquid electrolyte can absorb high-energy photons and can efficiently transfer the energy to the anchored near-infrared SD leading to an increase in optical absorption efficiency.[34] In another work, enhancement in photovoltaic device performance has been reported using long-range resonant energy transfer from a dissolved luminescent dopant confined in the interwire spaces of a nanowire array electrode to an acceptor species confined to the surface of the nanowires.[28]

In this contribution, we demonstrate that size tunable CdTe QDs capped with 3-mercaptopropionic acid (MPA), assembled in an N719-sensitized solar cell, can absorb visible light in the gaps where SD N719 has lower absorption or does not absorb any light. In this design, QDs serve as a cosensitizer which can directly transfer electrons to ZnO nanorods (NRs). Moreover, the QDs which are not in a direct attachment to the ZnO NR surfaces harvest the absorbed energy to nearby dye molecules via FRET rather than contribute directly as sensitizers. By using steady-state and picosecond-resolved fluorescence spectroscopy, we have demonstrated that photoluminescence (PL) from QDs can be useful to excite the SD molecule for an enhanced light absorption. The consequence of QD mediated electron and light-harvesting processes on the overall performance of a model QD-assembled DSSC has also been demonstrated.

2. EXPERIMENTAL SECTION

2.1. Materials. Analytical grade zinc acetate dihydrate, $(CH_3COO)_2Zn,2H_2O$ (Merck), zinc nitrate hexahydrate, $Zn(NO_3)_2{\cdot}6H_2O$ (Merck), and hexamethylenetetramine, $C_6H_{12}N_4$ (Aldrich), were used for the fabrication of ZnO NRs. Chloroplatinic acid ($H_2PtCl_6{\cdot}H_2O$), lithium iodide (LiI), and 4-tertbutylpyridine (TBP) were obtained from Fluka, and iodine (I_2) was obtained from Fisher Scientific. Fluorine-doped tin oxide (SnO_2: F) coated conducting glass substrates (FTO, 12Ω/square) from Nippon Sheet Glass, Japan, were purchased from Kintec, Hong Kong. Dye N719 was obtained from Solaronix, Switzerland. The precursors employed in this investigation to prepare CdTe QDs were sodium tellurite, Na_2TeO_3, and 3-mercaptopropionic acid, $HSCH_2CH_2CO_2H$, from Aldrich chemicals, cadmium chloride, $CdCl_2{\cdot}2.5H_2O$, sodium borohydride, $NaBH_4$, and trisodium citrate dehydrate, $C_6H_5Na_3O_7{\cdot}2H_2O$ from Merck. All chemicals were of analytical grade and were used without further purification.

2.2. Preparation of 3-MPA-Capped CdTe QDs. Several synthetic routes to CdTe QDs have been reported.[35−40] In this study, 0.12 mol of $CdCl_2$ was dissolved in 8 mL of deionized (DI) water, was diluted to 84 mL, and was stirred. To this solution 0.024 mol of trisodium citrate dihydrate, 0.03 mol of Na_2TeO_3 in 8 mL of DI water, 0.011 mol of 3-MPA, and 0.086 mol of $NaBH_4$ were added successively and were stirred to make the stock solution for CdTe QD synthesis. This stock solution was refluxed for 7, 20, and 30 min in a commercial Panasonic microwave oven (low-power mode) to synthesize 440, 500, and 550 nm absorption peak QDs, respectively. The QDs with 610 nm absorption peak were synthesized by refluxing the stock solution in a commercial oven at 106 °C for 9 h. The as-prepared QDs, without any further purification, were used in the fabrication of ZnO NR-based DSSCs.

2.3. Preparation of ZnO NRs. The most widely used fabrication method to obtain vertically aligned ZnO nanostructures is the hydrothermal method.[41−45] First, FTO substrates were cleaned ultrasonically with soap water, acetone, ethanol, and DI water. We dissolved 15 mM of zinc acetate dihydrate in 10 mL of DI water and sprayed this solution at a rate of 1 mL/min (from a distance of 25 cm) on top of the clean FTO substrates. The substrates were preheated to 420 °C on a hot plate before spraying. After spraying 10 mL completely, the substrates were allowed to cool to room temperature followed by annealing in air at 300 °C for 5 h.[46] The ZnO NPs seeded FTO substrates were then placed in a sealed chemical bath containing equimolar concentration of zinc nitrate hexahydrate and hexamethylenetetramine (20 mM) at 95 °C for 20 h. This leads to the growth of ZnO NRs of length ca. 3−4 μm, diameter 100−200 nm, and estimated surface coverage area of ∼62% as shown in Figure 1a. The ZnO NR coated substrates were then retracted from the chemical bath, were rinsed several times with DI water, and were annealed at 350 °C for 60 min to remove any organic impurities prior to further use.

2.4. Fabrication of QD-decorated Dye-Sensitized Solar Cells. CdTe QD decorated photoelectrodes (PEs) were fabricated by dipping the ZnO NR coated FTO into CdTe colloid at 60 °C for 3 h. The PEs were removed, were washed with ethanol, and were annealed at 165 °C for 1 h. This cycle was repeated three times to obtain a uniform layer of CdTe particles on the ZnO surface. For cosensitizing the PEs with N719 dye, the as-prepared CdTe QD coated PEs were dipped into a 0.5 mM dye N719 in ethanol solution for 24 h in dark at room temperature. After 24 h, the substrates were withdrawn from the dye solution and were rinsed with ethanol several times in order to remove the excess dye on the film surface. We define this geometry of the sample as ZnO-QD-N719. In another architecture, we have dipped the ZnO NR with N719 first, and then PEs were coated with CdTe QDs (ZnO-N719-QD architecture). The same procedures were

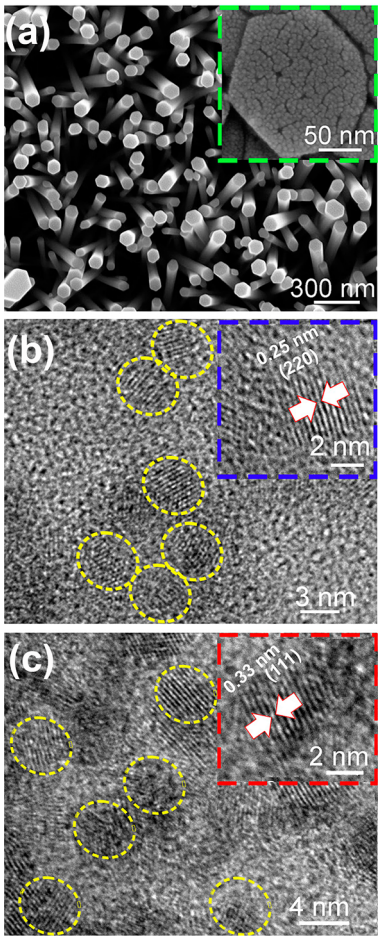

Figure 1. (a) Top-view SEM image of vertically aligned ZnO nanorods decorated on an FTO plate; the inset shows a closer view of hexagonal shaped ZnO NR on which CdTe QDs are attached. TEM images of (b) QD1 and (c) QD2 (two representative QDs) are shown; the insets show their corresponding HRTEM image.

followed to prepare the substrates for the time-resolved measurements also only by replacing FTO plates with quartz. PEs sensitized with N719 only (control) were fabricated by dipping ZnO PEs directly into 0.5 mM dye solution for 24 h following a similar procedure as described above. The PEs were then dried in dark at room temperature in a controlled humidity chamber (40% humidity) for 2 h. A thin layer of Pt catalyst deposited on the FTO substrates was used as a counter electrode to assemble the DSSC. The counter electrodes were prepared by dropping 10 μL of 5 mM chloroplatinic acid ($H_2PtCl_6{\cdot}H_2O$) solution in isopropanol on FTO substrates followed by the thermal decomposition of the $H_2PtCl_6{\cdot}H_2O$ to Pt NPs at 385 °C for 30 min. A single layer of Surlyn 1702 (50 μm thickness) from Dupont was placed between the two electrodes, and the device was sealed. The liquid electrolyte composed of the 0.5 M LiI, 0.05 M I_2, and 0.5 M 4-tert-butylpyridine (TBP) in acetonitrile (ACN) was then filled in the cell using capillary force through small holes drilled on the counter electrode. Finally, the holes in the counter electrode were sealed to prevent the electrolyte from leaking. In this respect, QDs are relatively less stable in iodine-based electrolyte,[47] and in the technological applications of this kind of QD-decorated solar cells, selection of other iodine-free electrolytes would be more appreciated. The charateristics of the solar cells reported here were recorded immediately after filling in the electrolytes in the sandwich structure in order to minimize losses due to corrosion of the CdTe QDs.[17]

2.5. Structural, Optical, and Electrical Characterization. Transmission electron microscopy (TEM) was carried out by applying a drop of the CdTe samples to carbon-coated copper grids. Particle sizes were determined from micrographs recorded at a magnification of 100 000× using an FEI (Technai TF 20, operating at 200 kV) instrument. A scanning electron microscope (SEM, JEOL JSM-6301F, operating at 20 kV) was used to study the morphology of the as-grown ZnO NRs. Steady-state absorption and emission spectra were measured with a Shimadzu UV-2450 spectrophotometer and Jobin Yvon Fluoromax-3 fluorimeter (pump power at 350 nm is ~0.663 mW/cm^2), respectively. All the photoluminescence transients were measured using picosecond-resolved time-correlated single-photon counting (TCSPC) technique, a commercially available picosecond diode laser-pumped (LifeSpec-ps) time-resolved fluorescence spectrophotometer from Edinburgh Instruments, United Kingdom. Picosecond excitation pulses from the picoquant diode laser were used at 375 nm with an instrument response function (IRF) of 60 ps. A microchannel plate photomultiplier tube (MCP-PMT, Hammamatsu) was used to detect the photoluminescence from the sample after dispersion through a monochromator. For all transients, the polarizer on the emission side was adjusted to 55° (magic angle) with respect to the polarization axis of the excitation beam. Photocurrent−voltage (J−V) characteristic measurements of the DSSC were performed under AM1.5G sun irradiation (100 mW/cm^2) using a 150 W small beam simulator (Sciencetech, model SF150).

2.6. Data Analysis. Curve fitting of observed fluorescence transients was carried out using a nonlinear least-squares fitting procedure to a function ($X(t) = \int_0^t E(t')R(t-t')\mathrm{d}t'$) comprised of convolution of the IRF ($E(t)$) with a sum of exponentials ($R(t) = A + \sum_{i=1}^{N} B_i e^{-t/\tau_i}$) with pre-exponential factors (B_i), characteristic lifetimes (τ_i), and a background (A). Relative concentration in a multiexponential decay is expressed as

$$c_n = \frac{B_n}{\sum_{i=1}^{N} B_i} \times 100$$

The average lifetime (amplitude-weighted) of a multiexponential decay[48] is expressed as

$$\tau_{av} = \sum_{i=1}^{N} c_i \tau_i$$

After the deconvolution, obtained time constants which are one-fourth of the IRF may be reliably reported within the signal-to-noise ratio of the fluorescence transients. We have estimated the standard errors in the lifetime data, FRET, and device parameters from repeated measurements. For the estimation of errors in the radii of different QDs, the standard deviation was calculated from the particle size distributions.

3. RESULTS AND DISCUSSION

Morphological characterization by SEM (Figure 1a) indicates the formation of arrays of ZnO NRs with a preferential growth direction along the polar facets in the [0002] direction of the ZnO hexagonal wurtzite crystal. The NRs growing perpendicular to the substrate are nearly uniform in length (~3 μm) and possess a characteristic hexagonal cross section with diameter of ~180 nm. The inset shows the magnified top view of a typical

dx.doi.org/10.1021/jp3046593 | J. Phys. Chem. C 2012, 116, 14248−14256

single NR decorated with CdTe QDs. Figure 1b and c shows the TEM images of two distinctly different sizes of CdTe QDs (QD1 and QD2) which are ~4 ± 0.2 and ~5 ± 0.4 nm in diameter. As shown in the insets of Figure 1b and c, high-resolution TEM (HRTEM) image reveals the fringes of CdTe with a lattice spacing of 0.33 and 0.25 nm corresponding to (111) and (220) planes of cubic CdTe crystal, which are in good agreement with previous reports.[49]

Both the absorption and photoluminescence (PL) spectra of CdTe QDs exhibit quantum size effect as shown in Figure 2.

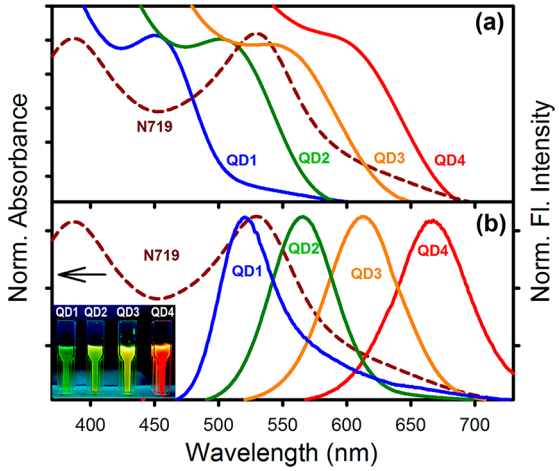

Figure 2. (a) Normalized absorption spectra of the sensitizing dye N719 and 3-MPA-capped CdTe QDs with average diameters of 4 nm (QD1), 5 nm (QD2), 7 nm (QD3), and 9 nm (QD4). (b) Significant overlap between absorption spectra of N719 and photoluminescence (PL) spectra of four different-sized CdTe QDs is shown.

The tunable absorption bands of CdTe QDs can be adjusted so that they preferentially cover the gaps of SD N719 absorption, that is, where SD has no or very low extinction coefficient (Figure 2a). As can be observed in Figure 2b, there are significant overlaps between the optical absorption of SD N719 and the emission bands of CdTe QDs, which is one of the foremost criteria for Förster resonance energy transfer (FRET) dynamics. As shown in Figure 3, upon 375 nm laser excitation, strong emissions of CdTe QDs (deposited on a quartz plate) were suppressed in the presence of SD N719. Herein, we propose FRET from donor CdTe QDs to N719 acceptor,[50] which is responsible for the observed suppression of the emission bands. The mechanism of FRET involves a donor in

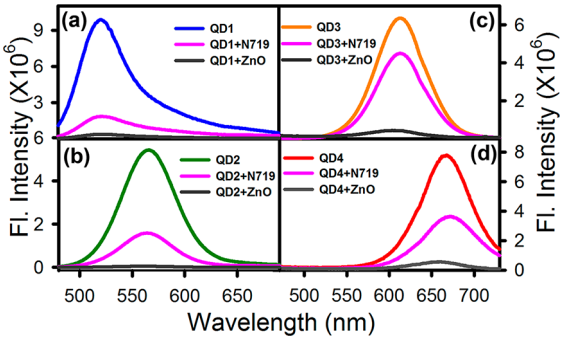

Figure 3. Steady-state emission quenching of different-sized CdTe QDs (a, QD1; b, QD2; c, QD3; d, QD4) in the presence of sensitizing dye N719 and ZnO nanorods. Excitation was at 375 nm.

an excited electronic state, which may transfer its excitation energy to a nearby acceptor in a nonradiative fashion through long-range dipole−dipole interaction.[48] The theory is based on the concept of treating an excited donor as an oscillating dipole that can undergo energy exchange with a second dipole having similar resonance frequency. In principle, if the fluorescence emission spectrum of the donor molecule overlaps the absorption spectrum of an acceptor molecule, and if the two are within a minimal distance from one another (1−10 nm), the donor can directly transfer its excitation energy to the acceptor via exchange of a virtual photon. The donor thus decays to the ground state while the acceptor is still excited. This results in the excitation of the acceptor from an indirect process, that is, the acceptor effectively captures photons that are not directly absorbed by it. The faster excited state lifetime of the CdTe-N719 composite with respect to that of the free QDs is clearly noticeable in Figure 4. Details of the spectroscopic parameters and the fitting parameters of the fluorescence decays are tabulated in Table 1.

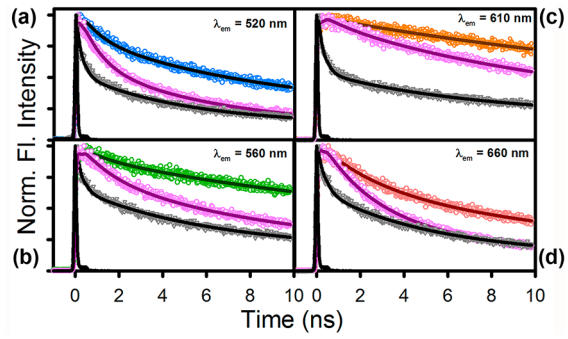

Figure 4. The picosecond-resolved fluorescence transients of four different-sized CdTe QDs (a, QD1; b, QD2; c, QD3; d, QD4) in the absence and presence of sensitizing dye N719 (pink) and ZnO nanorods (gray). The excitation wavelength was at 375 nm.

To estimate FRET efficiency of the donor (QDs) and hence to determine distances of donor−acceptor pairs, we followed the methodology described in chapter 13 of ref 48. The Förster distance (R_0) is given by

$$R_0 = 0.211 \times [\kappa^2 n^{-4} Q_D J(\lambda)]^{1/6} (\text{in Å}) \quad (1)$$

where κ^2 is a factor describing the relative orientation in space of the transition dipoles of the donor and acceptor. For donor and acceptors that randomize by rotational diffusion prior to the energy-transfer process, the magnitude of κ^2 is assumed to be $^2/_3$.[48,S1] The refractive index (n) of the medium is 1.4. The quantum yields (Q_D) of the donors in the absence of acceptor are measured with respect to a reference dye Rhodamine 123 (Q_D = 0.9) and are presented in Table 2. $J(\lambda)$, the overlap integral, which expresses the degree of spectral overlap between the donor emission and the acceptor absorption is given by

$$J(\lambda) = \frac{\int_0^\infty F_D(\lambda)\varepsilon_A(\lambda)\lambda^4 d\lambda}{\int_0^\infty F_D(\lambda) d\lambda} \quad (2)$$

where $F_D(\lambda)$ is the fluorescence intensity of the donor in the wavelength range of λ to $\lambda + d\lambda$ and is dimensionless. $\varepsilon_A(\lambda)$ is the extinction coefficient (in $M^{-1} cm^{-1}$) of the acceptor at λ. If λ is in nanometers, then $J(\lambda)$ is in units of $M^{-1} cm^{-1} nm^4$. Once

dx.doi.org/10.1021/jp3046593 | J. Phys. Chem. C 2012, 116, 14248−14256

Table 1. Dynamics of Picosecond-Resolved Luminescence Transients of CdTe QDs (QD1−QD4) in the Presence and Absence of SD N719 and ZnO NRs[a]

sample	observed wavelength	τ_1 (ns)	τ_2 (ns)	τ_3 (ns)	τ_{avg} (ns)	$k_{nr} \times 10^7$ (s^{-1})
QD1 (abs 445 nm)	520 nm	0.93 ± 0.03 (30%)	6.80 ± 0.15 (38%)	35.80 ± 0.45 (32%)	14.30 ± 0.21	
QD1 + N719	520 nm	0.90 ± 0.03 (40%)	4.80 ± 0.12 (38%)	23.40 ± 0.38 (22%)	7.30 ± 0.14	k_{FRET} = 6.70 ± 0.16
QD1 + ZnO	520 nm	0.21 ± 0.02 (61%)	4.20 ± 0.05 (25%)	21.30 ± 0.23 (14%)	4.20 ± 0.05	k_{PET} = 17.00 ± 0.40
QD2 (abs 500 nm)	560 nm	1.10 ± 0.15 (15%)	9.90 ± 0.78 (33%)	40.20 ± 0.95 (52%)	24.30 ± 0.77	
QD2 + N719	560 nm	1.20 ± 0.08 (25%)	7.50 ± 0.20 (43%)	34.90 ± 0.50 (32%)	14.70 ± 0.27	k_{FRET} = 2.60 ± 0.10
QD2 + ZnO	560 nm	0.21 ± 0.02 (52%)	4.70 ± 0.07 (25%)	26.20 ± 0.16 (23%)	7.30 ± 0.06	k_{PET} =10.00 ± 0.40
QD3 (abs 550 nm)	610 nm	0.84 ± 0.05 (3%)	16.20 ± 0.88 (45%)	43.60 ± 0.9 (52%)	29.90 ± 0.87	
QD3 + N719	610 nm	0.80 ± 0.08 (7%)	8.80 ± 0.27 (32%)	28.30 ± 0.68 (61%)	20.10 ± 0.51	k_{FRET} = 1.60 ± 0.03
QD3 + ZnO	610 nm	0.22 ± 0.07 (61%)	4.30 ± 0.12 (13%)	27.40 ± 0.14 (26%)	7.80 ± 0.02	k_{PET} = 9.50 ± 0.06
QD4 (abs 610 nm)	660 nm	2.35 ± 0.17 (27%)	8.10 ± 0.94 (36%)	31.80 ± 1.40 (37%)	15.30 ± 0.90	
QD4 + N719	660 nm	2.18 ± 0.06 (36%)	7.10 ± 0.30 (36%)	27.30 ± 1.00 (28%)	10.90 ± 0.41	k_{FRET} = 2.60 ± 0.07
QD4 + ZnO	660 nm	0.27 ± 0.02 (49%)	4.30 ± 0.50 (31%)	21.70 ± 0.13 (20%)	5.80 ± 0.19	k_{PET} = 10.70 ± 0.20

[a]The emission from CdTe QDs (emission at 520, 560, 610, and 660 nm) was detected with 375 nm laser excitation. k_{nr} represents nonradiative (FRET/PET) rate constant. The numbers in the parentheses indicate relative weightages.

Table 2. Various FRET Parameters[a] Obtained for Different-Sized CdTe QDs and SD N719

FRET pairs	$J(\lambda) \times 10^{14}$ (M^{-1} cm^{-1} nm^4)	Q_D	R_0 (nm)	E_{TR} (%)	r_{DA} (nm) from FRET	r (nm) from TEM
QD1 + N719	9.2 ± 0.2	0.18 ± 0.01	3.69 ± 0.05	0.490 ± 0.003	3.72 ± 0.03	2.00 ± 0.11
QD2 + N719	7.5 ± 0.3	0.29 ± 0.02	3.86 ± 0.07	0.400 ± 0.008	4.14 ± 0.06	2.50 ± 0.20
QD3 + N719	5.1 ± 0.2	0.45 ± 0.03	3.90 ± 0.07	0.330 ± 0.002	4.38 ± 0.08	3.50 ± 0.14
QD4 + N719	3.6 ± 0.1	0.40 ± 0.02	3.61 ± 0.04	0.290 ± 0.012	4.22 ± 0.04	4.50 ± 0.25

[a]Overlap integral ($J(\lambda)$), quantum yield (Q_D) in the absence of acceptor, Förster distance (R_0), FRET efficiency calculated from time-resolved study (E_{TR}), and donor−acceptor distance (r_{DA}) between the FRET pairs and radii (r) of QDs measured from TEM images.

the value of R_0 is known, the donor−acceptor distance (r) can be easily calculated using the formula

$$r^6 = \frac{[R_0^6(1 - E)]}{E} \quad (3)$$

Here, E is the efficiency of energy transfer. The transfer efficiency is measured using the relative fluorescence lifetime of the donor in the absence (τ_D) and presence (τ_{DA}) of the acceptor.

$$E = 1 - \frac{\tau_{DA}}{\tau_D} \quad (4)$$

From the average lifetime calculation for the CdTe−N719 adduct, we obtain the effective distance (using eqs 3 and 4) between the donor and the acceptor, r_{DA}, to be 3.72 ± 0.03, 4.14 ± 0.06, 4.38 ± 0.08, and 4.22 ± 0.04 nm for QD1−QD4, respectively. The insignificant variations in donor−acceptor distances compared to the radii of the QDs (measured from TEM image) can be rationalized from the fact that the origin of the PL arises essentially from surface states in the CdTe QDs.[17] Both degree of overlap and distance between donor and acceptor have been accounted simultaneously for FRET efficiency estimation. The energy-transfer efficiency from QD to N719 is observed to decrease with a subsequent decrease in overlap integral which is consistent with previous studies.[52,53] The calculated FRET parameters are also presented in Table 2.

Although FRET is an interesting phenomenon which requires neither physical contact nor charge exchange, direct attachment of the CdTe QDs with the ZnO NRs leads to photoinduced electron transfer (PET) from QDs to the conduction band of ZnO. Similar PET studies have been reported in the literature which is a fundamental process of QDSC that ultimately pilots a direct sensitization of the solar cell performance.[17,54,55] The rate of charge recombination, energy transfer, and charge injection processes (reactions i, ii, and iii, respectively) dictates the emission decay of CdTe QDs.

$$\mathrm{CdTe} + h\nu \rightarrow \mathrm{CdTe}(e + h) \rightarrow \mathrm{CdTe} + h\nu' \quad \text{(recombination)} \quad \text{(i)}$$

$$\mathrm{dye} + h\nu' \rightarrow \mathrm{dye}^* \quad \text{(energy harvesting)} \quad \text{(ii)}$$

$$\mathrm{CdTe}(e + h) + \mathrm{ZnO} \rightarrow \mathrm{CdTe}(h) + \mathrm{ZnO}(e) \quad \text{(electron harvesting)} \quad \text{(iii)}$$

Figure 4 shows the emission decay of CdTe QDs anchored to ZnO NR films on a quartz plate recorded with 375 nm diode laser excitation. As observed in the previous studies, both heterogeneity of samples and varying degree of surface defects introduce multiexponential decay behavior to the charge recombination process.[16,17] A significant decrease in QD lifetime, however, was observed in the presence of ZnO NRs. In particular, the fast component, which contributes nearly 61% of the decay, shows a major decrease in lifetime from 0.93 ± 0.03 to 0.21 ± 0.02 ns in the smallest QD−ZnO composite. The apparent rate constants, k_{nr}, were determined for the nonradiative processes by comparing the lifetimes of CdTe in the absence (τ_0) and in the presence (τ) of N719 and ZnO NRs using eq 5.

$$k_{nr} = 1/\langle\tau\rangle - 1/\langle\tau_0\rangle \quad (5)$$

For the smallest QD (i.e., QD1), the apparent rate constant for charge injection into ZnO NRs was estimated to be 1.7×10^8 s^{-1}, whereas the rate of energy transfer from QD1 to SD N719 is 6.7×10^7 s^{-1}. Therefore, it is evident that the charge injection from the excited CdTe to the ZnO NRs occurs with a rate constant that is an order of magnitude higher than that of energy transfer between CdTe and N719. The above

dx.doi.org/10.1021/jp3046593 | J. Phys. Chem. C 2012, 116, 14248−14256

estimation of average lifetimes takes into account both short- and long-lived components. A major population of the charge injection process occurs with a greater rate constant (as high as 10^9 s^{-1}) if we compare only the fast component of the emission transients. For example, ~61% of the emission decay of CdTe QDs on ZnO surface occurs with a lifetime of 0.21 ± 0.02 ns indicating that the major fraction of the charge injection event occurs on an ultrafast time scale.

To investigate the mechanism of cosensitization of CdTe QDs in the layered architectures (Figure 5a, b) related to DSSC

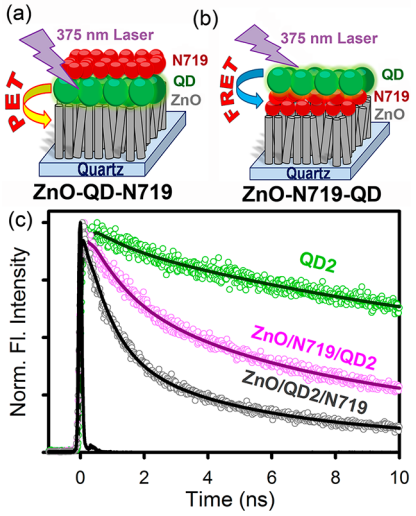

Figure 5. Two different architectures of CdTe QD decorated dye-sensitized ZnO nanorod substrates, namely, (a) ZnO−QD−N719 and (b) ZnO−N719−QD. (c) The picosecond-resolved fluorescence transients of CdTe QD2 showing PET and FRET in two different architectures. The excitation wavelength was 375 nm and the emission was monitored at 560 nm.

fabrication, picosecond-resolved fluorescence study was performed (Figure 5c). The fluorescence transient of the bare QDs not in the vicinity of N719 or ZnO is shown in the figure as a reference. In the ZnO−QD−N719 architecture (Figure 5a), QDs are sandwiched between ZnO NRs and N719. In these conditions, QDs can either directly transfer electrons to the conduction band (CB) of ZnO NRs or can nonradiatively transfer energy to SD N719. The fluorescence decay parameters, as shown in Table 3, are comparable to the distinct lifetimes of an electron-transfer process (Table 1). Therefore, the picosecond-resolved fluorescence transient of CdTe QDs in the ZnO−QD−N719 architecture reveals a direct injection of charge carriers from QDs to ZnO NRs via PET. The role of the capping ligands of the colloidal QDs has been demonstrated to have paramount importance on the efficient charge separation at the QD/polymer interface.[56] In this respect, the electron-transfer pathway is found to prevail over the FRET process with short-chain 3-MPA ligands associated to CdTe QDs. In the other architecture, ZnO−N719−QD (Figure 5b), the QDs are separated by a layer of N719 molecules from the ZnO NRs whereby light harvesting could only occur through FRET from QDs to N719. It is being conventional that the N719 dye binds the ZnO by using its carboxylic groups;[57] as a result, the residual chains of N719 are free and are away from the ZnO, which allows them to interlace with the 3-MPA ligands of the QDs via efficient hydrophilic interactions. This sort of an association results in an average distance between the donor and the acceptor, which lies within the Förster radius and allows an efficient energy transfer. The assorted lifetimes (Table 3) of the QDs in this particular configuration are comparable to the decay parameters of the energy-transfer route (as shown in Table 1) which reveals that an additional indirect excitation of N719 can be introduced by using the sensitivity of FRET, and this type of engineered solar cells should contribute to higher photocurrents. The nonradiative rate constants (k_{nr}) in these two architectures, as presented in Table 3, are almost analogous to the k_{nr} values of the individual systems that lead to either energy- or electron-transfer pathways (Table 1).

The effectiveness of QD decoration in solar cell performance was evaluated by employing them in a photoelectrochemical cell with two different architectures (Figure 5a, b) as discussed previously. The use of CdTe QDs as a sensitizer in photoelectrochemical cells has been investigated by several research groups.[17,27,58,59] DSSC devices fabricated with N719 dye as sensitizer in the presence and the absence of CdTe QDs (QD1 and QD2) were characterized by wavelength-dependent photocurrent spectroscopy (Figure 6a, b) and photocurrent−voltage (J−V) measurements (Figure 6c); the resulting photovoltaic parameters are summarized in Table 4. The wavelength-dependent photocurrent is the number of electrons collected under known photon intensity that was evaluated from the short-circuit photocurrent (J_{sc}) measured for different incident wavelengths (λ). The inset of Figure 6a shows the wavelength-dependent incident power of the monochromator. The photocurrent versus wavelength plot of the ZnO−QD−N719 architecture is presented in Figure 6a which shows a spectral response in the range of 350−750 nm. In devices without any modification of the dye sensitizer with QDs, the broad photocurrent spectrum is attributed to the photogenerated charge carrier in SD N719.[28] As shown in the figure, the presence of QD1 (abs. = 440 nm) and QD2 (abs. = 500 nm) in the sensitization process leads to a dramatic increase in the photocurrent in the spectral region of blue photons indicating the occurrence of a direct injection of electrons from QDs to ZnO NRs similar to the observations made by the picosecond-resolved fluorescence studies (Figure 5c). In this case, dye (N719) loading was lower in ZnO−QD−N719

Table 3. Dynamics of Picosecond-Resolved Luminescence Transients of CdTe QDs (QD1−QD4) in the Presence and Absence of SD N719 and ZnO NRs[a]

sample	observed wavelength	τ_1 (ns)	τ_2 (ns)	τ_3 (ns)	τ_{avg} (ns)	$k_{nr} \times 10^7$ (s^{-1})
QD2 (abs 500 nm)	560 nm	1.10 ± 0.15 (15%)	9.90 ± 0.78 (33%)	40.20 ± 0.95 (52%)	24.30 ± 0.77	
ZnO−N719−QD2	560 nm	1.20 ± 0.18 (33%)	7.00 ± 0.65 (45%)	32.00 ± 0.86 (22%)	10.60 ± 0.54	5.30 ± 0.31
ZnO−QD2−N719	560 nm	0.72 ± 0.09 (59%)	4.50 ± 0.45 (33%)	22.80 ± 0.82 (8%)	7.30 ± 0.27	9.60 ± 0.38

[a]The emission from CdTe QD (emission at 560 nm) was detected with 375 nm laser excitation. Numbers in the parentheses indicate relative weightages.

dx.doi.org/10.1021/jp3046593 | J. Phys. Chem. C 2012, 116, 14248−14256

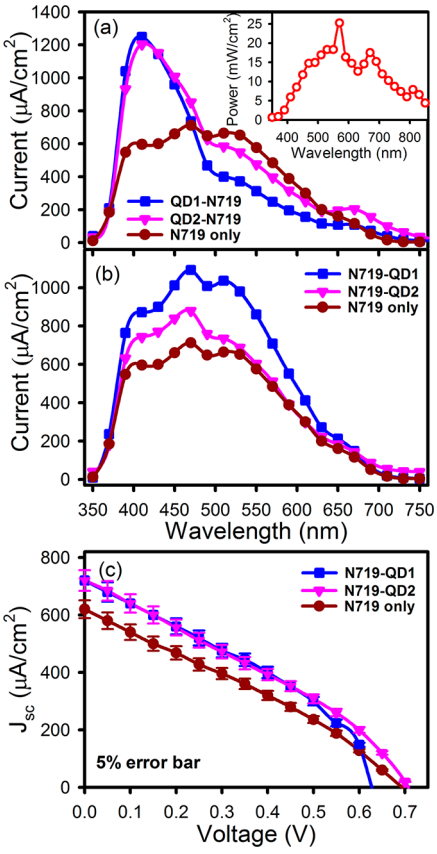

Figure 6. Photocurrent vs wavelength spectra for DSSCs comprised of (a) ZnO−QD−N719 and (b) ZnO−N719−QD architectures, respectively. The inset shows incident power vs wavelength plot. (c) Photocurrent−voltage (J−V) characteristics for ZnO−N719−QD architecture.

Table 4. Device Performance[a] of the Dye-Sensitized Solar Cells Made of Two Different Architectures of QD Loading

device with N719	V_{OC} (V)	J_{SC} (μA/cm^2)	FF (%)	η (%)
ZnO−N719−QD1	0.63 ± 0.04	720 ± 36	35.27 ± 2.70	0.16 ± 0.01
ZnO−N719−QD2	0.71 ± 0.03	720 ± 29	30.99 ± 1.31	0.16 ± 0.01
ZnO−N719	0.69 ± 0.05	620 ± 33	29.92 ± 0.50	0.13 ± 0.01

[a]Short-circuit photocurrent densities (J_{sc}/cm^2), open-circuit voltage (V_{oc}), fill factor (FF), and efficiency (η).

architecture compared to that of ZnO−N719 assembly because of prior attachment of QD to the ZnO NRs. Therefore, at 530 nm (maximum optical absorption in N719), the photocurrent was found to be lower in ZnO−QD−N719 compared to ZnO−N719 system. Hence, a fair comparison of wavelength-dependent photocurrent and overall device performance of these architectures is not likely when the amounts of dye present in different architectures are not similar. For a better assessment, we engineered devices with similar dye loading in ZnO−N719−QD and ZnO−N719 solar cells. The ZnO−N719−QD architecture shows increased photocurrent (Figure 6b) compared to ZnO−N719 system throughout the spectral region as additional photogenerated charge carriers from N719 dye (via FRET) adds up to the net photocurrent. Figure 6c shows the J−V characteristics of solar cells with ZnO−N719−QD architecture as compared to solar cells sensitized with dye only. The fill factor (FF) and power conversion efficiency (η) of the solar cells can be determined from eqs 6 and 7

$$\mathrm{FF} = V_M J_M / V_{OC} J_{SC} \quad (6)$$

$$\eta = V_{OC} J_{SC} / \mathrm{FF} \quad (7)$$

where J_{sc} and V_{oc} are the short-circuit current density and the open-circuit voltage; V_M and J_M are the voltage and current density at the maximum power output, respectively. As shown in Table 4, the calculated values of FF and the overall power conversion efficiency of ZnO−N719 based DSSCs are found to improve in the presence of QD assembly. Overall, the analysis of photodevice data in the measured ZnO−N719−QD configuration reflects similarly the cosensitization of CdTe QDs tagged with the sensitivity of FRET as observed by the picosecond-resolved fluorescence study (Figure 5c).

The photoconductivity measurement[32] of the ZnO NR, ZnO−N719, and ZnO−N719−QD thin films were carried out in order to better understand the contribution of QDs via FRET to the net photocurrent in the devices. At a fixed bias voltage of 2.5 V, the photocurrent across the thickness of the thin films was measured by utilizing FTO as one of the electrodes and a small (4 mm diameter) drop of mercury (Hg) on top of the film as a counter electrode (as shown in Figure 7a). The light source (intensity = 25 mW cm^{-2}) was turned on

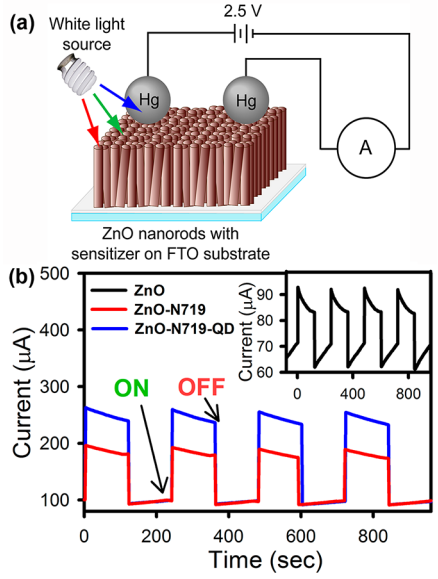

Figure 7. (a) Schematic representation of photoconductivity measurement setup by using FTO as one of the electrodes and a small (4 mm diameter) drop of mercury (Hg) on top of the film as a counter electrode. (b) Photocurrent responses of ZnO NRs (inset), ZnO−N719, and ZnO−N719−QD2 arrays under bias voltage of 2.5 V. The photocurrent was measured across the thickness of the films with 25 mW cm^2 incident power from a halogen light source.

and off every 120 s, and the obtained current values were continuously recorded using a programmable multimeter (Gwinstek GDM-396). Figure 7b shows the photocurrent response for the ZnO NR (inset), ZnO−N719, and ZnO−N719−QD2 thin films. An improved photocurrent was observed for the ZnO−N719−QD2 thin film (~260 μA) under illuminated conditions compared to the ZnO−N719 thin

dx.doi.org/10.1021/jp3046593 | J. Phys. Chem. C 2012, 116, 14248−14256

Scheme 1. Dual-Sensitization in QD-decorated DSSCs[a]

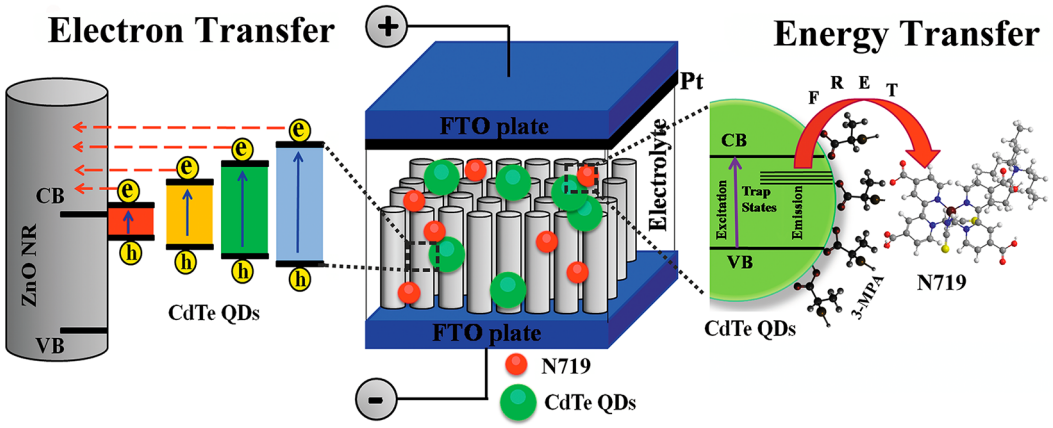

[a]The system consists of a fluorinated tin oxide (FTO) on which semiconductor ZnO NR (gray cylinder) is fabricated. The sensitizer dye N719 (small red circle) and 3-MPA-capped CdTe QDs (big green circle) are bound to ZnO NR by surface adsorption. The directly attached QDs lead to sensitization via efficient charge injection from excited semiconductor nanocrystal, CdTe into ZnO NR. Moreover, the QDs which are within the close proximity of sensitizing dye N719 introduce an additional indirect excitation of N719 by using the sensitivity of FRET. The upshot of the above dual-sensitization mode is found to be reflected in the overall solar cell performance.

film (~190 μA). This shows that an additional indirect excitation of N719 can be obtained by decorating the dye molecules with CdTe QDs. For the model DSSCs prepared with the same arrangement of ZnO−N719−QD, we observed a similar enhancement of photocurrent (Figure 6c) in the presence of CdTe QDs which further confirms the contribution of FRET toward the improvement of efficient energy harvesting in dual-sensitized solar cells.

4. CONCLUSIONS

In conclusion, by using spectroscopic techniques, we have demonstrated the utilization of dual-sensitization in DSSCs as schematically represented in Scheme 1. The steady-state and the time-resolved luminescence measurements on 3-MPA-capped CdTe QDs reveal the size-dependent charge injection characteristics of ZnO photoelectrodes. The QDs which are not in a direct contact with the semiconductor can harvest visible light which resonantly transfer to SD N719 and offer an indirect excitation of the SD. To investigate the improvement of light-harvesting because of QD decoration in a DSSC, wavelength-dependent photocurrent, photocurrent−voltage (J−V) characteristics, and photoconductivity measurements were performed for both the QD-assembled and reference (only sensitizing dye) devices. The cosensitization in the presence of CdTe QDs leads to a significant increment in photocurrent throughout the visible spectral region and also enhances the short-circuit current density as additional photogenerated charge carriers from N719 dye (via FRET) adds up to the net photocurrent. As we continue to modify, study, and improve such FRET pair sensitizers, the realization of truly inexpensive, stable, and efficient DSSCs grows nearer.

AUTHOR INFORMATION

Corresponding Author

*E-mail: skpal@bose.res.in.

Notes

The authors declare no competing financial interest.

ACKNOWLEDGMENTS

S.S. thanks UGC (India) and A.M. thanks CSIR (India) for fellowships. We thank DST (India) for financial grants SR/SO/BB-15/2007. K.L., T.B., and J.D. would like to acknowledge partial financial support from the National Nanotechnology Center belonging to the National Science & Technology Development Agency (NSTDA), Ministry of Science and Technology (MOST), Thailand, and the Centre of Excellence in Nanotechnology at the Asian Institute of Technology, Thailand. We thank Mr. Samik Roy Moulik for performing TEM measurements on CdTe QDs.

REFERENCES

(1) O'Regan, B.; Grätzel, M. *Nature* **1991**, *353*, 737−740.
(2) Grätzel, M. *Nature* **2001**, *414*, 338−344.
(3) Nazeeruddin, M. K.; Angelis, F. D.; Fantacci, S.; Selloni, A.; Viscardi, G.; Liska, P.; Ito, S.; Takeru, B.; Grätzel, M. *J. Am. Chem. Soc.* **2005**, *127*, 16835−16847.
(4) Nazeeruddin, M. K.; Klein, C.; Liska, P.; Grätzel, M. *Coord. Chem. Rev.* **2005**, *249*, 1460−1467.
(5) Martinson, A. B. F.; Elam, J. W.; Hupp, J. T.; Pellin, M. J. *Nano Lett.* **2007**, *7*, 2183−2187.
(6) Yum, J. H.; Walter, P.; Huber, S.; Rentsch, D.; Geiger, T.; Nüesch, F.; Angelis, F. D.; Grätzel, M.; Nazeeruddin, M. K. *J. Am. Chem. Soc.* **2007**, *129*, 10320−10321.
(7) Burke, A.; Schmidt-Mende, L.; Ito, S.; Grätzel, M. *Chem. Commun.* **2007**, 234−236.
(8) Campbell, W. M.; Jolley, K. W.; Wagner, P.; Wagner, K.; Walsh, P. J.; Gordon, K. C.; Schmidt-Mende, L.; Nazeeruddin, M. K.; Wang, Q.; Grätzel, M.; et al. *J. Phys. Chem. C* **2007**, *111*, 11760−11762.
(9) Fan, S. Q.; Cao, R. J.; Xi, Y. X.; Gao, M.; Wang, M. D.; Kim, D. H.; Kim, C. W.; Ko, J. J. *Optoelectron. Adv. Mater.* **2009**, *3*, 1027−1033.
(10) Yu, W. W.; Qu, L.; Guo, W.; Peng, X. *Chem. Mater.* **2003**, *15*, 2854−2860.
(11) Kamat, P. V. *J. Phys. Chem. C* **2007**, *111*, 2834−2860.
(12) Zhang, Q.; Guo, X.; Huang, X.; Huang, S.; Li, D.; Luo, Y.; Shen, Q.; Toyoda, T.; Meng, Q. *Phys. Chem. Chem. Phys.* **2011**, *13*, 4659−4667.
(13) Ruhle, S.; Shalom, M.; Zaban, A. *Chem. Phys. Chem.* **2010**, *11*, 2290−2304.
(14) Shalom, M.; Ruhle, S.; Hod, I.; Yahav, S.; Zaban, A. *J. Am. Chem. Soc.* **2009**, *131*, 9876−9877.

(15) Kamat, P. V. *J. Phys. Chem. C* **2008**, *112*, 18737−18753.
(16) Kongkanand, A.; Tvrdy, K.; Takechi, K.; Kuno, M.; Kamat, P. V. *J. Am. Chem. Soc.* **2008**, *130*, 4007−4015.
(17) Bang, J. H.; Kamat, P. V. *ACS Nano* **2009**, *3*, 1467−1476.
(18) Ross, R. T.; Nozik, A. J. *J. Appl. Phys.* **1982**, *53*, 3813−3818.
(19) Schaller, R. D.; Agranovich, V. M.; Klimov, V. I. *Nat. Phys.* **2005**, *1*, 189−194.
(20) Schaller, R. D.; Klimov, V. I. *Phys. Rev. Lett.* **2004**, *92*, 186601.
(21) Kamat, P. V.; Tvrdy, K.; Baker, D. R.; Radich, J. G. *Chem. Rev.* **2010**, *110*, 6664−6688.
(22) Shalom, M.; Dor, S.; Ruhle, S.; Grinis, L.; Zaban, A. *J. Phys. Chem. C* **2009**, *113*, 3895−3898.
(23) Shalom, M.; Albero, J.; Tachan, Z.; Martínez-Ferrero, E.; Zaban, A.; Palomares, E. *J. Phys. Chem. Lett.* **2010**, *1*, 1134−1138.
(24) Etgar, L.; Park, J.; Barolo, C.; Lesnyak, V.; Panda, S. K.; Quagliotto, P.; Hickey, S. G.; Nazeeruddin, M. K.; Eychmuller, A.; Viscardi, G.; et al. *RSC Adv.* **2012**, *2*, 2748−2752.
(25) Choi, H.; Nicolaescu, R.; Paek, S.; Ko, J.; Kamat, P. V. *ACS Nano* **2011**, *5*, 9238−9245.
(26) Giménez, S.; Rogach, A. L.; Lutich, A. A.; Gross, D.; Poeschl, A.; Susha, A. S.; Mora-Seró, I.; Lana-Villarreal, T.; Bisquert, J. *J. Appl. Phys.* **2011**, *110*, 014314.
(27) Ruland, A.; Schulz-Drost, C.; Sgobba, V.; Guldi, D. M. *Adv. Mater.* **2011**, *23*, 4573−4577.
(28) Shankar, K.; Feng, X.; Grimes, C. A. *ACS Nano* **2009**, *3*, 788−794.
(29) Buhbut, S.; Itzhakov, S.; Tauber, E.; Shalom, M.; Hod, I.; Geiger, T.; Garini, Y.; Oron, D.; Zaban, A. *ACS Nano* **2010**, *4*, 1293−1298.
(30) Buhbut, S.; Itzhakov, S.; Oron, D.; Zaban, A. *J. Phys. Chem. Lett.* **2011**, *2*, 1917−1924.
(31) Makhal, A.; Sarkar, S.; Bora, T.; Baruah, S.; Dutta, J.; Raychaudhuri, A. K.; Pal, S. K. *J. Phys. Chem. C* **2010**, *114*, 10390−10395.
(32) Sarkar, S.; Makhal, A.; Bora, T.; Baruah, S.; Dutta, J.; Pal, S. K. *Phys. Chem. Chem. Phys.* **2011**, *13*, 12488−12496.
(33) Siegers, C.; Hohl-Ebinger, J.; Zimmermann, B.; Würfel, U.; Mülhaupt, R.; Hinsch, A.; Haag, R. *Chem. Phys. Chem.* **2007**, *8*, 1548−1556.
(34) Hardin, B. E.; Hoke, E. T.; Armstrong, P. B.; Yum, J. H.; Comte, P.; Torres, T.; Frechet, J. M. J.; Nazeeruddin, M. K.; Grätzel, M.; McGehee, M. D. *Nat. Photonics* **2009**, *3*, 406−411.
(35) Rogach, A. L.; Franzl, T.; Klar, T. A.; Feldmann, J.; Gaponik, N.; Lesnyak, V.; Shavel, A.; Eychmuller, A.; Rakovich, Y. P.; Donegan, J. F. *J. Phys. Chem. C* **2007**, *111*, 14628−14637.
(36) Gaponik, N.; Talapin, D. V.; Rogach, A. L.; Hoppe, K.; Shevchenko, E. V.; Kornowski, A.; Eychmuller, A.; Weller, H. *J. Phys. Chem. B* **2002**, *106*, 7177−7185.
(37) Wuister, S. F.; Swart, I.; Driel, F. V.; Hickey, S. G.; Donegaa, C. D. M. *Nano Lett.* **2003**, *3*, 503−507.
(38) Brennan, J. G.; Siegrist, T.; Carroll, P. J.; Stuczynski, S. M.; Reynders, P.; Brus, L. E.; Steigerwald, M. L. *Chem. Mater.* **1990**, *2*, 403−409.
(39) Murray, C. B.; Norris, D. J.; Bawendi, M. G. *J. Am. Chem. Soc.* **1993**, *115*, 8706−8715.
(40) Aldeek, F.; Balan, L.; Medjahdi, G.; Roques-Carmes, T.; Malval, J. P.; Mustin, C.; Ghanbaja, J.; Schneider, R. *J. Phys. Chem. C* **2009**, *113*, 19458−19467.
(41) Baruah, S.; Dutta, J. *Sci. Technol. Adv. Mater.* **2009**, *10*, 013001.
(42) Fang, X.; Zhang, L. *J. Mater. Sci. Technol.* **2006**, *22*, 1−18.
(43) Fang, X.; Bando, Y.; Gautam, U. K.; Ye, C.; Golberg, D. *J. Mater. Chem.* **2008**, *18*, 509−522.
(44) Kim, K. S.; Jeong, H.; Jeong, M. S.; Jung, G. Y. *Adv. Funct. Mater.* **2010**, *20*, 3055−3063.
(45) Fang, X.; Hu, L.; Ye, C.; Zhang, L. *Pure Appl. Chem.* **2010**, *82*, 2185−2198.
(46) Bora, T.; Kyaw, H. H.; Sarkar, S.; Pal, S. K.; Dutta, J. *Beilstein J. Nanotechnol.* **2011**, *2*, 681−690.
(47) Li, L.; Yang, X.; Gao, J.; Tian, H.; Zhao, J.; Hagfeldt, A.; Sun, L. *J. Am. Chem. Soc.* **2011**, *133*, 8458−8460.
(48) Lakowicz, J. R. *Principles of Fluorescence Spectroscopy*, 2nd ed.; Kluwer Academic/Plenum Publishers: New York, 1999.
(49) Pehnt, M.; Schulz, D. L.; Curtis, C. J.; Jones, K. M.; Ginley, D. S. *Appl. Phys. Lett.* **1995**, *67*, 2176−2178.
(50) Mora-Sero, I.; Gross, D.; Mittereder, T.; Lutich, A. A.; Susha, A. S.; Dittrich, T.; Belaidi, A.; Caballero, R.; Langa, F.; Bisquert, J.; et al. *Small* **2010**, *6*, 221−225.
(51) Watrob, H. M.; Pan, C. P.; Barkley, M. D. *J. Am. Chem. Soc.* **2003**, *125*, 7336−7343.
(52) Li, M.; Cushing, S. K.; Wang, Q.; Shi, X.; Hornak, L. A.; Hong, Z.; Wu, N. *J. Phys. Chem. Lett.* **2011**, *2*, 2125−2129.
(53) Batabyal, S.; Makhal, A.; Das, K.; Raychaudhuri, A. K.; Pal, S. K. *Nanotechnology* **2011**, *22*, 195704.
(54) Robel, I.; Kuno, M.; Kamat, P. V. *J. Am. Chem. Soc.* **2007**, *129*, 4136−4137.
(55) Mora-Sero, I.; Bisquert, J.; Dittrich, T.; Belaidi, A.; Susha, A. S.; Rogach, A. L. *J. Phys. Chem. C* **2007**, *111*, 14889−14892.
(56) Martínez-Ferrero, E.; Albero, J.; Palomares, E. *J. Phys. Chem. Lett.* **2010**, *1*, 3039−3045.
(57) Ruankham, P.; Macaraig, L.; Sagawa, T.; Nakazumi, H.; Yoshikawa, S. *J. Phys. Chem. C* **2011**, *115*, 23809−23816.
(58) Aga, R. S., Jr.; Jowhar, D.; Ueda, A.; Pan, Z.; Collins, W. E.; Mu, R.; Singer, K. D.; Shen, J. *Appl. Phys. Lett.* **2007**, *91*, 232108.
(59) Cao, X.; Chen, P.; Guo, Y. *J. Phys. Chem. C* **2008**, *112*, 20560−20566.